JOURNAL OF MATERIALS SCIENCE 6 (1971) 998–1006

Growth of Graphite Single Crystals from Iron-Carbon Solutions

C. ROSCOE, D. NAGLE, S. B. AUSTERMAN*
Department of Materials Science, Pennsylvania State University, University Park, Penna. 16802, USA
**Autonetics, 3370 Miraloma Avenue, Anaheim California, 93803, USA*

Graphite crystals grown from hypereutectic solutions of carbon in iron were examined microscopically with a view to establishing the mechanisms of growth. It is proposed that nucleation occurred on a second phase which had been retained in some crystals extracted from the molten solution. The perfection of the crystals, which is compared with that of naturally occurring and pyrolytic graphites, is a function of the extent of decomposition of this second phase and the impurity content of the melt.

1. Introduction

The need for large, defect-free, graphite single crystals becomes continually more pressing as experiments designed to reveal the physico-chemical properties of graphite increase in sophistication. The notion that the dissolution of carbon in certain one- or multi-component melts would lead to graphite formation is far from being a novel idea. However, before the advent of the studies of Austerman *et al* [1] little was known concerning the precise conditions necessary for formation of well developed single crystals. Now that this barrier has been at least partially removed, it has become expedient to unravel the mechanisms responsible for crystal growth. Through such studies it may be possible in the future to suitably modify the existing techniques to improve both the perfection and dimensions of the extracted crystals.

The more recent innovations concerning the solution growth of graphite single crystals have been reviewed by Austerman [2]. Although different workers have utilised a wide variety of elements for the growth medium, iron and nickel have emerged as perhaps the most widely used. The present discussion will be restricted merely to the consideration of crystals extracted from hypereutectic Fe-C solutions, as growth from nickel, for instance, has been found to occur by significantly different modes [3]. In the vast majority of instances the crystals grown from Fe-C solutions adopted a thin platelet habit, the larger specimens having typical dimensions of $2 \times 1 \times 0.02$ cm, although columnar crystals were also observed.

2. Experimental

2.1. Growth Conditions

The growth conditions relating to the crystals investigated here have been described previously [4], so only the most pertinent points will be reiterated. The essential criteria for the development of crystals possessing the desired quality were considered to be a slow growth rate at a limited number of nucleation sites. The first criterion was satisfied by employing low supersaturations of carbon, estimated to be 2 to 3%, which were promoted either by slow cooling or by the establishment of a temperature gradient across the melt. The temperatures employed were commonly in the region of 1100 to 1500°C. Compliance with the second criterion was made by avoiding the use of carbon to construct the growth vessel. The only carbon allowed to come into contact with the melt was the block intended for dissolution.

The possibility of impurities affecting crystal growth was minimised by utilising pure iron (99.9%) and spectroscopically pure graphite. In addition to residual impurities, some further contamination of the melts probably arose from slight dissolution of both the alumina crucible employed as a growth vessel and a calcia-stabilised zirconia baffle submerged in the melt in some runs. In later experiments the zirconia was replaced by alumina.

In all, a series of twenty-seven individual attempts were made to grow the desired crystals from iron and nickel melts [4]. The crystals to be described here were derived from the experiments identified as G2 and G27. G2 represents growth from an iron melt with a relatively rapid cooling rate, the crystals being removed from the frozen ingot, whereas in G27 the crystals were grown during slow cooling and subsequently removed from the molten iron. In both instances the crystals were completely submerged in the iron during crystal growth, except for a few in G2 that were exposed by contraction of the cooling melt. An atmosphere of N_2–10% CO or Ar–10% CO was introduced into the furnace to prevent oxidation of the charge.

2.2. Examination of the Crystals

The graphite crystals were investigated under both an optical microscope, which could be fitted with either interference contrast equipment or a polarisation interferometer, and a scanning electron microscope. The possible presence of certain specific impurity elements in the crystals was sought in an electron microprobe analyser with a 2 μm spot size. Attempts to determine the nature of a second phase sometimes observed in the crystals were made with an X-ray diffractometer. Transmission electron microscopy and diffraction, as well as glancing angle electron diffraction, were carried out at an accelerating voltage of 75 kV.

3. Growth Mechanisms

3.1. Spiral Growth

The character of the predominant crystal habit suggests that a spiral growth mechanism [5] played no more than a minor role in the growth process. This viewpoint was corroborated by examination of the more perfectly formed crystals under both the optical and electron microscopes. Only occasional spiral growth steps were found and symmetrical examples such as that shown in fig. 1 were extremely rare. This is perhaps contrary to expectation considering the density, 10^3 cm^{-2}, of non-basal screw dislocations traversing the fully developed crystals and the low carbon supersaturation required to promote growth.

It is pertinent to record here that a small minority of the G2 crystals possessed a greater than normal ratio of thickness to diameter, viz. 1:10. Closer inspection of these crystals revealed that their surfaces exhibited considerable terracing, which bore no apparent relationship to non-basal screw dislocations. It is believed that this enhanced growth rate along the *c*-axis resulted from the precipitation of carbon from an austenite phase towards the end of the growth experiment.

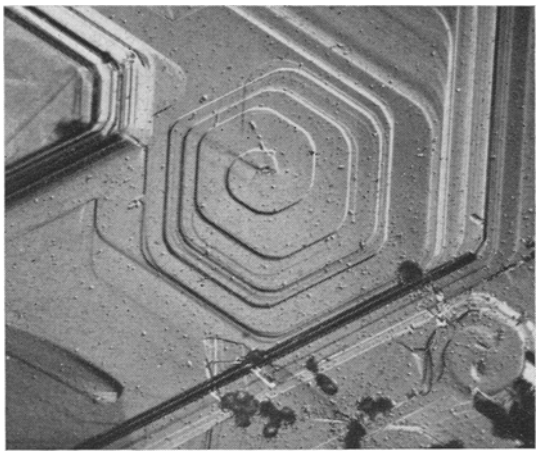

Figure 1 Symmetrical growth spiral centred on a non-basal screw dislocation (× 170).

3.2. Nucleation of a Second Phase

3.2.1. Identification of Second Phase

Cleavage of G27 crystals very occasionally exposes another phase co-existing with the graphite lattice. Fig. 2a provides evidence for two such second-phase particles, ABCD and EFG, implanted in a graphite crystal. These particles exhibit a number of noteworthy features. For the vast majority of observed examples, the projection of the interface between the two phases lies along either $\langle 10\bar{1}0 \rangle$ or $\langle 11\bar{2}0 \rangle$ directions in the basal plane of the graphite host lattice. Further, despite the often high propensity for twinning in the surrounding graphite matrix, there is no evidence of recognisable twins in the co-existing phase. Both backscattered electron micrographs and X-ray fluorescent micrographs taken in the electron microprobe analyser indicated the co-existing phase to be richer in iron than carbon. The X-ray fluorescence pattern shown in fig. 2b was obtained from the particle ABCD (see fig. 2a) with the spectrometer tuned for iron.

Efforts were made to identify this iron-carbon phase by X-ray diffraction. After many attempts, a sample was eventually prepared, by a process of successive cleavage, in which the second phase

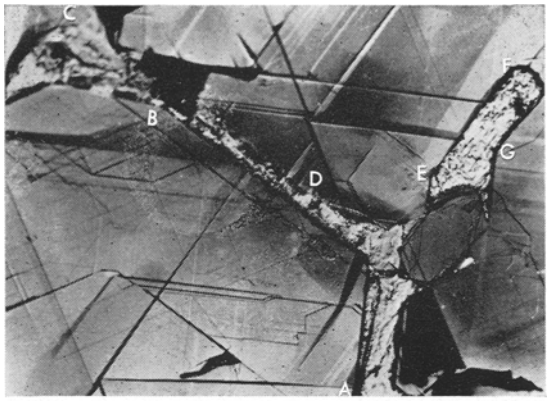

(a)

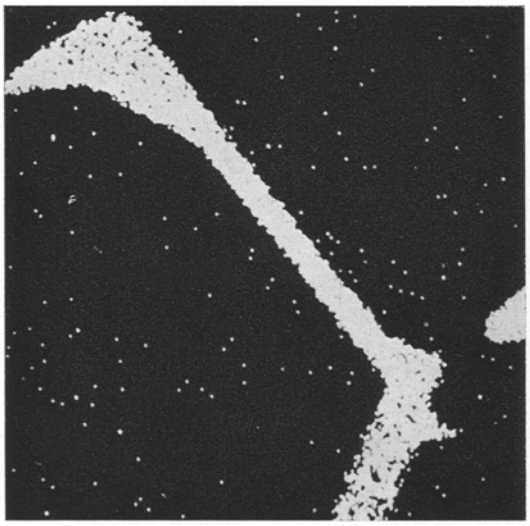

(b)

Figure 2 (a) Crystallites ABCD and EFG represent a second-phase co-existing with the graphite matrix (× 310). (b) X-ray fluorescent micrograph indicating the high iron content of the crystallite ABCD (fig. 2a) (× 310)

constituted as much as 5 to 10% of the crystal surface under examination. Despite this, the resulting diffraction pattern from the entire sample was identical with the pattern from a purified Ticonderoga graphite crystal.

Subsequently the graphite crystal partially depicted in fig. 2a was thinned to such a degree that it began to break up. In this manner it was possible to isolate a crystal fragment partially bounded by the second phase. This fragment was then mounted on the reflection stage of the electron microscope and a series of both glancing angle and transmission diffraction patterns were obtained. The latter originated from a sufficiently thin portion of the second phase which had been fortuitously bent out of the plane of the bulk sample. (The thickness of the bulk sample was for the most part appreciably greater than 1000 Å.)

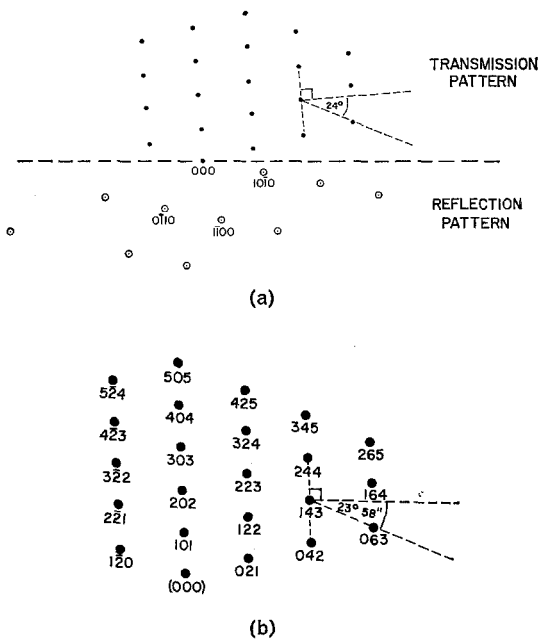

Figure 3 (a) Composite electron diffraction pattern obtained from the second phase. (b) Schematic representation of the reciprocal plane corresponding to a [$\bar{2}\bar{1}2$] pole of cementite.

The diffraction pattern presented schematically in fig. 3a is actually a composite of two patterns, which were superimposed on the same photographic plate, one formed by transmission through the second phase and the other by reflection from both the second phase and the graphite matrix. The presence of the graphite pattern is important sinceit provided an internal standard for an accurate determination of the diffraction constant of the microscope. This constant was used to determine the interplanar distances presented in tableI which pertain to the transmission portion of the pattern. These calculated values correspond closely to the series of planes for the cementite lattice [6-9] listed in table I, which have the [$\bar{2}\bar{1}2$] direction as a common pole and, therefore, lie in the [$\bar{2}\bar{1}2$] reciprocal lattice shown in fig. 3b.

A probable explanation for the X-ray diffrac-

TABLE I

Observed interplanar distances (Å)	Some interplanar distances in the cementite lattice (Å)	Indices of corresponding planes
3.73	3.76	(101)
2.38	2.38	(021)
2.25	2.20	($\bar{1}$20)
1.82	1.85	(122)
1.65	1.61	($\bar{2}2\bar{1}$)

tion data lies in the fact that all the strong reflections expected from the cementite lattice are nearly coincident with reflections observed from graphite alone.

The cementite cleavage surfaces shown in fig. 2a are typically decorated by tiny agglomerates of iron formed by slight decomposition occurring within the bulk phase. Under the microscope, some of the particles exhibited a red colouration indicating that the iron had acted as a getter for small traces of oxygen in the system and had become, at least, partially oxidised. (It is well known that the affinity of iron for oxygen is greater than that of graphite basal planes [10].) Podgurski *et al* [11] during a study of the disproportionation of carbon monoxide over iron, concluded that traces of oxygen, sufficient to form only a few layers of magnetite, can apparently stabilise the cementite structure. This would seem to suggest that the oxygen content of the iron melt might influence the rate of formation and/or decomposition of cementite during the crystal growth experiments.

3.2.2. Relative Orientations

It was observed (e.g. fig. 2a) that the cleavage crack within a cementite region remained parallel to the graphite cleavage – that is, the plane of the cementite coincident with the {000*l*} plane of graphite is a cleavage plane. Merely from consideration of the interplanar spacings in cementite it is expected that the latter will be {100}. Notably, Maurer and Warrington [7] found that cementite plates extracted from deformed pearlite possessed a predominantly (001) orientation and, moreover, that they occasionally exhibited cleavage fractures along (100) planes. The cementite/graphite interface was stated earlier to project along ⟨10$\bar{1}$0⟩ and ⟨11$\bar{2}$0⟩ directions of the graphite lattice. In cognisance of these points a relationship is proposed in table II between the cementite and graphite lattices, the *a*,*b*, and *c* axes of cementite being assumed parallel to the [01$\bar{1}$0], [$\bar{2}$110] and *c*-axes of graphite, respectively.

TABLE II Proposed orientation relationship between cementite and graphite

Cementite Direction	Interlayer spacings (Å) (7)	Graphite (a = 2.4614 Å) Direction	Equivalent spacings (Å)	% mismatch
a-axis [100]	4.5144	[01$\bar{1}$0]	$\sqrt{3}\,a$ 4.2635	5.78 across 4 bonds
b-axis [010]	5.0787	[$\bar{2}$110]	2 *a* 4.9228	3.15 across 4 bonds
c-axis [001]	6.7297	*c*-axis [0001]	6.707	0.31

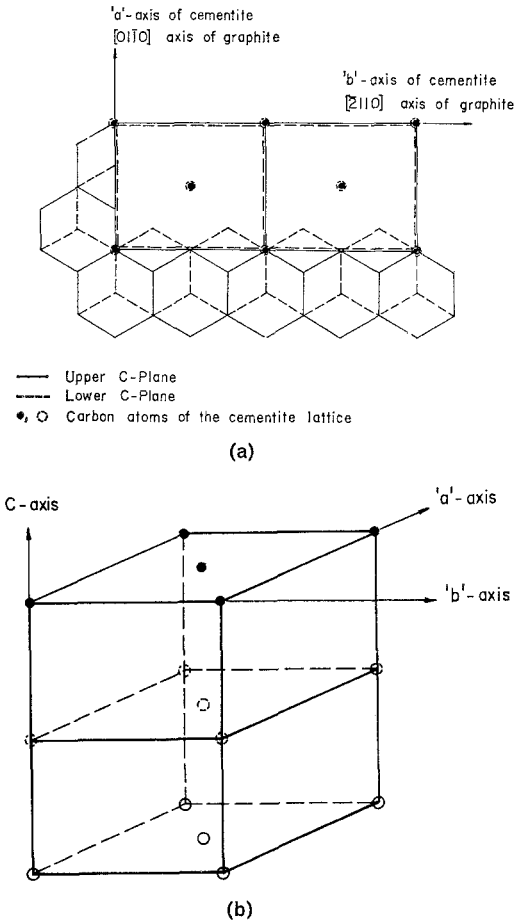

Figure 4 (a) Proposed structural relationship between the cementite and graphite lattices. (b) Body-centred orthorhombic array of carbon atoms in the cementite lattice.

The simplest atomic arrangement for the

common interface between the two phases, consistent with this relationship, is schematically depicted in fig. 4a. The interface lies parallel to the *c*-axis of both the cementite and graphite lattices which are perpendicular to the plane of this drawing. It has been assumed that the carbon atoms of the two lattices remain coplanar across the interface. The body-centred orthorhombic array of carbon atoms associated with cementite, plus tie lines, is presented in fig. 4b for comparative purposes.

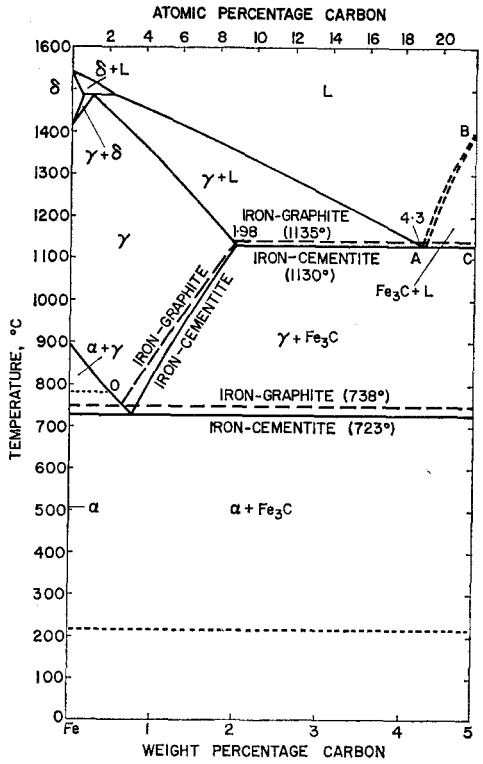

Figure 5 Iron-carbon phase diagram, taken from reference [12].

3.2.3. Precipitation of Cementite from Solution

The experimental conditions pertaining to the initiation of crystal growth correspond to those described by the hypereutectic portion of the Fe-C phase diagram [12] (fig. 5). In this region of the phase diagram, graphite is shown as the stable equilibrium solid phase and cementite as a non-equilibrium phase. This is in agreement with the work of Darken and Gurry [13] who presented data to show that, at all temperatures above the eutectic temperature, cementite was thermodynamically unstable relative to graphite.

The cementite we observe is attributed to the kinetics of nucleation in a slightly non-equilibrium system. In accord with this, Noda *et al* [14] found rapid cooling of a carbon-saturated melt led to the formation of substantial concentrations of cementite in the absence of silicon. Arguments based on the premise that the cementite we observe formed as a result of the freezing of an Fe-C solution, engulfed in the graphite crystals as the latter cooled through the eutectic temperature, are not tenable on two counts: (i) Some of the cementite seed crystals completely traversed the thickness of graphite crystals removed from the melt before the eutectic temperature was reached. (ii) Cementite was never observed in G2 crystals, which were not extracted from solution before solidification occurred.

Unfortunately, there have been relatively few other studies concerned with the initial precipitation of a solid phase from a saturated Fe-C solution. However, at least two pieces of evidence have been presented which suggest that cementite nuclei could indeed form at lower supersaturations than grapite crystals. First, the solubility of carbon in molten iron is extensive and might exceed 25 at. % [15] which corresponds with the composition Fe_3C. It has been deduced from this that moecular aggregates of Fe_3C can exist in the liquid [15]: consequently little redistribution of components would be necessary for precipitation of cementite as a transitional or metastable phase. Some studies supporting this conclusion are reviewed by Epstein [16].

Persistence of the precipitated cementite phase, which results in its retention in a few G27 crystals, is believed in part to be attributable to the formation of a fairly strong metal-carbon bond in the case of iron [15]. (Following the work of Darken and Gurry [13], cementite retention is also favoured by the substantial decrease in the degree of metastability of cementite, relative to graphite, as the temperature is lowered through the eutectic temperature.) In contrast to iron, for both cobalt and nickel the metal-carbon bond is much weaker and graphitisation can occur almost immediately. This leads directly to the second point suggesting that cementite could precipitate directly from solution: namely, evidence has been obtained [17] for the existence in solution of the considerably less stable hypereutectic nickel carbide, Ni_3C, at temperatures of 1400°C.

3.2.4. Growth from Cementite Seeds

In view of the foregoing discussion, it is considered that the platelet crystals grown in both experiments G2 and G27 were nucleated on the prismatic faces of cementite crystals, precipitated from solution with an {001} needle axis. (Regions originally occupied by cementite were readily identified in the G2 crystals.) As a result of the anisotropic character of the bonding in graphite, the crystal thickness is determined, in the absence of other growth mechanisms, by the thickness of the cementite seed.

It is pertinent to note that in Si-Fe melts, where cementite formation is suppressed, Baraniecki *et al* [18] have entertained the notion that graphite nucleation occurs on the hexagonal form of silicon carbide.

4. Crystal Perfection

4.1. Comparison with Naturally Occurring and Pyrolytic Graphites

Apart from the presence of twins, extensive regions of cleaved G2 and G27 crystals appeared perfect under the optical microscope. Unlike Ticonderoga crystals of comparable dimensions, there was no tendency toward sub-division of the crystals by arrays of non-basal screw dislocations.

Under the electron microscope the crystals were indistinguishable from Ticonderoga crystals. Predominantly single crystal diffraction patterns were obtained, although the presence of twist boundaries [19] was noted. The concentration of vacancies was below the limits of detection possible by the gold decoration technique [20], i.e. $< 10^5$ cm^{-2}, and no non-basal screw dislocations having a Burgers vector < 100 Å were found. From this standpoint the crystals are vastly superior to most pyrolytic graphites, which also have the disadvantage of a comparatively small crystalline size, between 1 to 10^3 μm. Electron microscopy failed to detect any difference in perfection across those G2 crystals which became only partially embedded in the freezing ingot and those entirely immersed. But X-ray diffraction rocking curves [2] did reveal a greater incidence of tilt boundaries [21] in those portions immersed in the ingot.

It was, however, a characteristic of G2 and G27 crystals that they each contained at least one region, normally constituting only a small proportion of the total crystal volume, disrupted on a macroscopic scale. Some typical examples are presented in sections 4.2 and 4.3.

4.2. Decomposition of Cementite

In all G2 and many G27 crystals examined, the cementite seed crystals had begun to decompose above the eutectic temperature. As a result of this reaction the cementite had been replaced, to differing extents (figs. 6a to d), by graphite.

Fig. 6a provides a typical example of the structure formed during decomposition. The predominantly triangular graphite plates possess a common orientation, their sides defining $\langle \bar{2}110 \rangle$ directions in the host crystal, implying that the cementite had existed in single crystal form. (Electron microprobe analysis indicated that the material appearing in darker contrast was iron.) In the region PQRS (Fig. 6b), revealed by cleaving a G27 crystal, cementite decomposition had been initiated at an earlier stage in the experiment. Consequently, intergrowth of the plates has occurred by addition of carbon atoms from the bulk solution. The outlines of some of the larger plates formed during this process are still visible, giving the secondary graphite lattice (i.e. the one replacing cementite) a mosaic appearance. Note that in this particular example a small amount of cementite (labelled C) has been retained within the crystal bulk. Other examples were observed, again in cleaved crystals, where the secondary graphite was for the most part indistinguishable from the remainder of the crystal. But post-growth oxidation did reveal that a majority of the non-basal screw dislocations traversing the crystals were contained in the secondary graphite. This could account for the lack of growth spirals (section 3.1).

The secondary graphite lattice never completely fills the volume originally occupied by the cementite crystal. However, the cavities left in most of the extracted crystals had been at least partially overgrown by graphite plates extending from the surrounding lattice (figs. 6c and d). Deformation of these plates appeared to be the principle cause for the formation of the leaf twins which were a prominent feature of many growth surfaces. The inclination of the twins to the latter was most commonly $20° 50' \pm 5'$, as measured on a two-circle optical goniometer. In the example given in fig. 6c only one twin, T, has formed, although complex twins arrangements were found. The twin shown in fig. 6d has become completely engulfed by the crystal. At this stage the twins provide re-entrant edges capable of perpetuating growth in the *c*-direction.

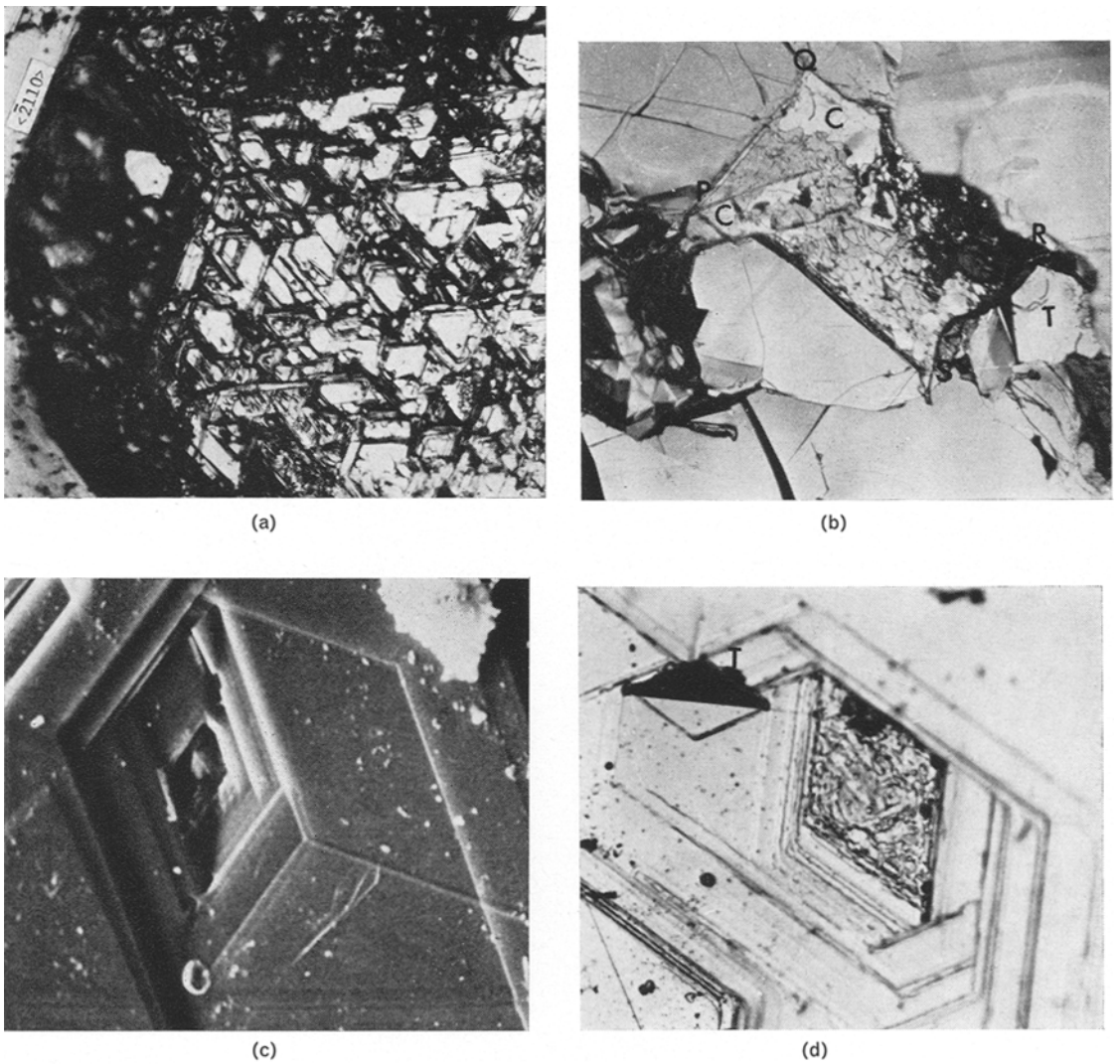

Figure 6 (a) Structure formed during decomposition of cementite (× 400). (b) The graphite lattice within the region PQRS was formed by intergrowth of plates similar to those in fig. 6a (× 240). (c) Scanning electron micrograph of a partially overgrown cavity resulting from decomposition of a cementite crystal (× 2500). (d) Final form of a leaf twin, T, nucleated in the manner shown in figure 6c (× 160).

4.3. Spheroidal Carbon

The perfection of some G2 crystals was impaired by the presence of spheroidal carbon. Often the latter was contained in a compact layer held within the crystal bulk. The hexagonal facets resolved on some of the larger spheroids (fig. 7a) suggest that the latter each consisted of a graphite lattice sub-divided by a network of tilt boundaries [21]. This type of structure apparently allows the spheroids to transform into graphite platelets [22, 23] such as those lying within the circular inclusion in fig. 7b. When this transformation occurred in a compact layer of spheroids it resulted in the formation of a thin graphite film. The example shown in fig. 7c was found on both matched faces of a cleaved G2 crystal. The cracks did not occupy corresponding positions in the two portions and so were presumably formed as the film cleaved.

Spheroidal particles adhering to prismatic and pyramidal faces (fig. 8a) also occasionally became trapped within the crystal bulk. Subsequent transformation of these spheroids to platelets left a series of voids lying chiefly along $[10\bar{1}0]$

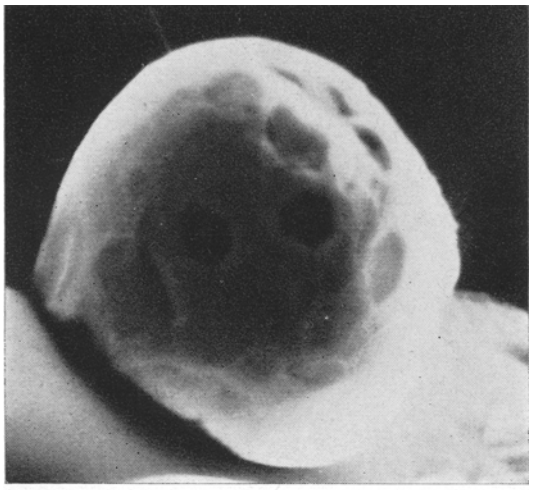

(7a)

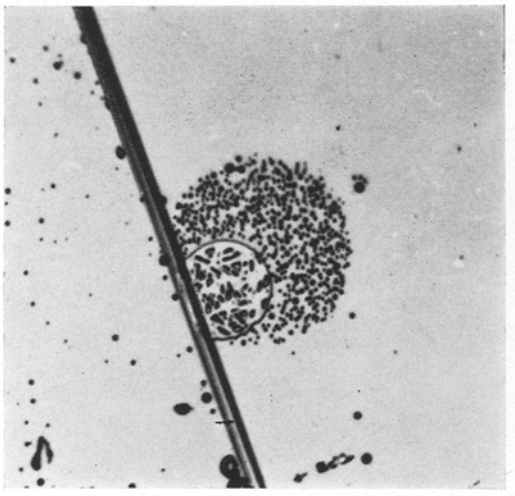

(7b)

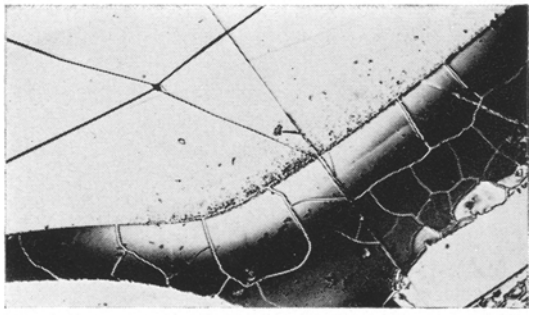

(7c)

Figure 7 (a) Scanning electron micrograph of spheroidal graphite particle (× 9000). (b) The platelets held within the circular inclusion appear to have formed by rearrangement of spheroidal particles (× 500). (c) Graphite film resulting from the intergrowth of tiny platelets such as those in fig. 7c (× 280).

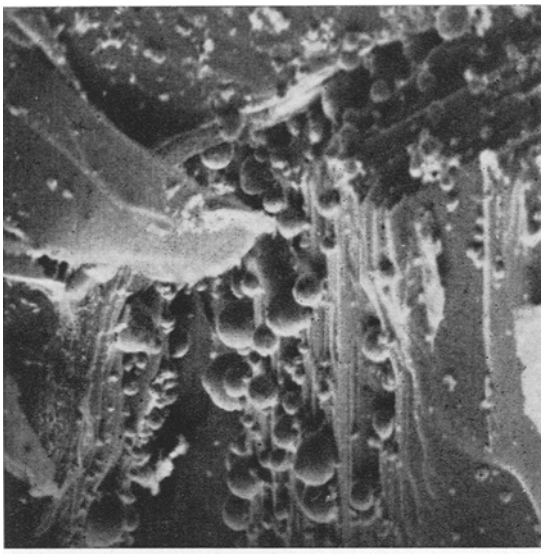

(a)

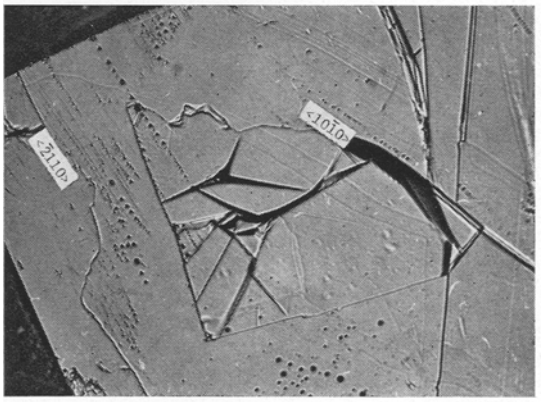

(b)

Figure 8 (a) Scanning electron micrograph of spheroidal particles adhering to adjacent prismatic growth faces (× 1200). (b) Arrays of tiny inclusions, each decorated by an iron particle, found in a cleaved G2 crystal (× 190).

planes (fig. 8b). Many of these voids were decorated by a tiny particle of iron, the implication being that the iron was originally held at the centre of each spheroid in the manner described by Oberlin *et al* [22].

5. Conclusions

The precipitation of cementite crystals from hypereutectic Fe-C solutions was the first event to occur during the cooling cycle of the growth

experiments. These crystals then acted as favourable sites for the nucleation of graphite crystals. Despite the initial presence of cementite, and sometimes spheroidal carbon, the crystals were superior in quality to both Ticonderoga crystals and stress-recrystallised pyrolytic graphites, cementite being eventually replaced in the crystals by single crystal graphite.

Acknowledgements

The authors are most grateful to Professor P. L. Walker, Jr. for his advice and encouragement throughout this work and also acknowledge helpful discussions with D. Gibbon. The work was supported by the Atomic Energy Commission on Contract No. AT(30–1) – 1710.

References

1. S. B. AUSTERMAN, S. M. MYRON, and J. W. WAGNER, *Carbon* **5** (1967) 549.
2. S. B. AUSTERMAN, "The Chemistry and Physics of Carbon", Volume 4 (Marcel Dekker, New York 1968) p. 137.
3. C. ROSCOE, D. NAGLE, and S. B. AUSTERMAN. (To be published.)
4. S. B. AUSTERMAN, J. W. WAGNER, and S. M. MYRON, *U.S.A.E.C. Report* NAA-SR-12486(1968).
5. F. C. FRANK, *Discuss Faraday Soc.* **5** (1949) 48.
6. H. LIPSON and N. J. PETCH, *J. Iron Steel Inst.* **142** (1940) 95.
7. K. MAURER and D. H. WARRINGTON, *Phil. Mag.* **15** (1967) 321.
8. A. I. GARDIN, *Soviet Physics Cryst.* 7 (1963) 694.
9. E. J. FASISKA and G. A. JEFFREY, *Acta Cryst.* **19** (1965) 463.
10. J. M. THOMAS and P. L. WALKER, JR. *Carbon* **2** (1965) 434.
11. H. H. PODGURSKI, J. T. KUMMER, T. W. DEWITT, and P. H. EMMETT, *J. Amer. Chem. Soc.* **72** (1950) 5382.
12. A.S.M. "Metals Handbook", p. 1182.
13. L. S. DARKEN and R. W. GURRY, *J. Metals* **3** (1951) 1015.
14. T. NODA, Y. SUMIYOSHI, and N. ITO, *Carbon* **6** (1969) 813.
15. H. J. GOLDSCHMIDT, "Interstitial Alloys" (Plenum Press 1967) p. 114.
16. S. EPSTEIN, "Alloys of Iron and Carbon" (McGraw-Hill, New York 1936) p. 151.
17. H. MORROGH and W. J. WILLIAMS, *J. Iron Steel Inst.* **155** (1947) 321.
18. C. BARANIECKI, P. H. PINCHBECK, and F. B. PICKERING, *Carbon* **7** (1969) 213.
19. G. K. WILLIAMSON, *Proc. Roy. Soc. London* **A257** (1960) 459.
20. G. R. HENNIG, "The Chemistry and Physics of Carbon", Volume 2 (Marcel Dekker, New York 1966) p. 1.
21. R. BACON and R. SPRAGUE, "Direct Observations of Imperfections in Crystals" (Interscience, New York 1962) p. 357.
22. A. OBERLIN, F. ROUSSEAUX, and J. P. ROUCHY, 18th Reunion de La Société de Chemie Physique, Paris (June 1968), p. 160.
23. I. E. BOLOBOV, *Fiz. Metall. i Metallov*, **20** (1965) 258.

Received 3 February 1970 and accepted 28 March 1971.